DALTON
FULL PAPER

Crystal supramolecularity. Multiple phenyl embraces by $[PPN]^+$ cations †

Gareth R. Lewis * and Ian Dance

School of Chemistry, University of New South Wales, Sydney 2052, Australia.
E-mail: gareth.lewis@unsw.edu.au

Received 28th September 1999, Accepted 30th November 1999

Analysis of the 752 crystals in the Cambridge Structural Database containing $[Ph_3PNPPh_3]^+$ ($[PPN]^+$) cations has revealed mutually attractive interactions between the cations leading to the formation of supramolecular motifs. The cation is flexible due to P–N–P bending: calculation of single point energies for an idealised $[H_3PNPH_3]^+$ fragment show a flat energy well for the cation, with there being less than 1 kcal mol^{-1} difference in energy between P–N–P angles of 130–180°. The most populated conformation is that with a P–N–P angle in the range 140–145°. The types of inter-cation interaction can be classified by a combination of the N–P · · · P angle, the N–P · · · P–N torsion angle and the four intermolecular P · · · P distances between neighbouring cations. Interactions with an N–P · · · P angle of greater than 125° indicate a sixfold phenyl embrace (6PE), whilst those at more acute angles form expanded phenyl embraces with neighbouring cations either parallel (PEPE) or orthogonal (OEPE). The PEPE and OEPE are differentiated by torsion angle or intermolecular P · · · P separations. Computation of the energies of attraction between the cations gives values in the ranges 7.0–10.5, 7.9–11.1 and 8.6–13.0 kcal mol^{-1} for the 6PE, OEPE and PEPE respectively. The individual embraces combine to form zigzag chains of cations leading to either columnar or layered structures. The crystal lattice formed does not depend on anion size or charge.

Introduction

The focus of supramolecular chemistry is to identify and understand the attractive intermolecular forces that determine the aggregation of molecules in the condensed phase. The intention is to exploit these interactions to manufacture materials with desirable and controllable physical characteristics, such as optical, electronic and magnetic properties.[1] Molecular crystals are infinite supramolecular assemblies[2] and analysis of the crystallographic data in the Cambridge Structural Database[3] allows the recognition of prevalent supramolecular motifs.

Analysis of the crystal packing of $[PPh_4]^+$ cations recognised the widespread occurrence of multiple phenyl embraces, in which individual intermolecular phenyl–phenyl attractive interactions combine with significant net attraction.[4–10] Multiple phenyl embraces are characterised by (a) the participation of two or more phenyl groups from each neighbouring molecule, (b) geometrical concertedness, and (c) strong attraction. The more common multiple phenyl embraces are the sixfold phenyl embrace, 6PE, containing six edge-to-face (**ef**) attractions, and two types of fourfold phenyl embrace, or 4PE. The two common 4PEs are distinguished by the angle between the two C_{ipso}–P–C_{ipso} planes; the parallel fourfold phenyl embrace (P4PE) has these two planes approximately parallel whereas the orthogonal fourfold phenyl embrace (O4PE) has these planes approximately orthogonal. In the O4PE the four phenyl rings engage in four **ef** interactions, whilst the P4PE comprises one offset-face-to-face (**off**) and two **ef** interactions.[5] The net attractive energies for the 6PE are calculated to be in the range 8–11 kcal mol^{-1}, comparable with the energies of the stronger hydrogen bonds. Analogous multiple aryl embraces are observed involving the heteroaromatic rings in $[M(bipy)_3]^{z+}$[11] and $[M(terpy)_2]^{z+}$[12] complexes. The multiple phenyl embraces between $[PPh_4]^+$ cations combine to form 2- and 3-D networks in the crystal lattice with hexagonal arrays and zigzag infinite chains of 6PEs,[9] and ladders and layers of 4PEs.[10]

While the $[PPh_4]^+$ cation is popular with synthetic chemists endeavouring to crystallise anions, equally so is the bis(triphenylphosphoranylidene)ammonium cation, $[Ph_3PNPPh_3]^+$ ($[PPN]^+$), especially in the crystallisation of large organometallic anions. The tendency for salts containing $[PPN]^+$ to form crystalline solids could arise from analogous multiple phenyl embraces between cations in the solid state. The very low osmotic and ionic activity coefficients of $[PPN]^+$ salts in water suggest that $[PPN]^+$ cations form dimers at low concentrations,[13] indicating that the cations can form supramolecular assemblies.

In this paper we analyse the crystal packing of salts containing $[PPN]^+$ cations, and define the multiple phenyl embrace motifs between them. The geometries and the calculated energies of these supramolecular motifs for $[PPN]^+$ cations are reported, as well as the patterns of their occurrence and formation of extended networks in molecular crystals.

Methodology

Version 5.17a (May 1999 release) of the Cambridge Structural Database[3] was searched for molecules containing $[PPN]^+$ cations. This initial set was analysed according to the P · · · P separation. Disordered and unreliable ($R_1 > 0.10$) structures were excluded. The reduced set was then analysed according to the N–P · · · P angle, which revealed the broad classes of interaction and the number of structures in each class (see ESI). The data were analysed using the Cambridge Quest3D graphical software and the program InsightII.[14]

Intermolecular energies E were calculated as the sum of the interatomic energies,[15,16] using the Lennard-Jones 6–12 interatomic potential for attractive and repulsive van der Waals energies E^{vdw}_{ij}, and the coulombic components $E^{coulombic}_{ij}$ [eqns. (1)–(5)]. The atom partial charges q_i were obtained from a QEq calculation,[17] using the CERIUS^2 software.[18] The computed

† Electronic supplementary information (ESI) available: refcodes and geometrical parameters. See http://www.rsc.org/suppdata/dt/a9/a907808h/

Table 1 Parameters used in the calculations of interatomic energies: see eqns. (3), (4) and (5)

Atom type	r^a_i/Å	e^a_i/kcal mol^{-1}	q_i
ipso-C in phenyl ring	1.95	0.093	0.05
Other ring C	1.95	0.093	−0.10
All H in phenyl ring	1.60	0.020	0.13
P	2.10	0.200	0.00
N	2.05	0.065	−0.20

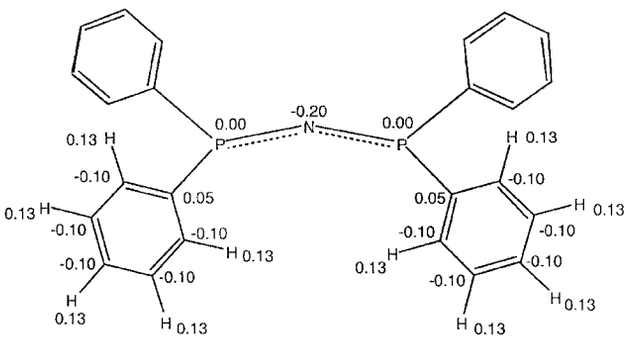

Fig. 1 Partial charges for the $[PPN]^+$ cation used for the computation of pairwise intermolecular interaction energies.

$$E = \Sigma E_{ij} \quad (1)$$

$$E_{ij} = E^{vdw}{}_{ij} + E^{coulombic}{}_{ij} \quad (2)$$

$$E^{vdw}{}_{ij} = e^a{}_{ij}\,[(d_{ij}/d^a{}_{ij})^{-12} - 2(d_{ij}/d^a{}_{ij})^{-6}] \quad (3)$$

$$d^a{}_{ij} = (r^a{}_i + r^a{}_j),\ e^a{}_{ij} = (e^a{}_i e^a{}_j)^{0.5} \quad (4)$$

$$E^{coulombic}{}_{ij} = q_i q_j/\varepsilon d_{ij} \quad (5)$$

partial charges sum to +1 for each $[PPN]^+$ cation, and therefore the mutual repulsion due to like charges is explicitly included in the net energies as calculated. The parameters and charges used in eqns. (1) to (5) are presented in Table 1 and Fig. 1: d_{ij} is the interatomic separation; $e^a{}_{ij}$ and $d^a{}_{ij}$ are respectively the energy and the interatomic distance for the attractive well of the vdW potential;[19] and the permittivity ε was set equal to d_{ij}.[19] As in our previous work,[10,11,20] the parameters $e^a{}_i$, $r^a{}_i$ and q_i for the intermolecular potential E have been adjusted to reproduce the best experimental and theoretical data on intermolecular energies, and to be consistent with periodic variations of charge and polarisability for the various atom types.[21]

Density functional calculations were performed with the program DMol,[22] using the 'blyp' functional which incorporates gradient corrections, and using double numerical polarised basis sets. Volumes were computed using a Connolly surface[23] with a probe sphere of radius 1.4 Å, using the CERIUS^2 software.[18]

Results and discussion

For the 752 crystal structures in the CSD containing $[PPN]^+$ cations a histogram of intermolecular P···P distance gave a maximum between 6.6–7.0 Å, falling to a minimum at approximately 7.2 Å, before increasing at distances above 7.3 Å. Of these 752 structures, 131 were discarded for being disordered or crystallographically unreliable ($R_1 > 0.10$). Owing to the distribution in the histogram, the 139 structures with a P···P separation of less than 7.25 Å were selected, denoted the 'motif set'.

Chemical diversity of $[PPN]^+$ salts

The majority of structures contain large organometallic metal carbonyl clusters, such as $[Os_5(\mu_5\text{-}C)(\mu\text{-}CO)(CO)_{13}]^{2-}$ (CSD refcode CASRAP), or carboborane cluster complexes, such as $[Rh_2(\mu\text{-}Br)(PPh_3)_2(NH_2)_2(\eta\text{-}B_{10}CH_{10})_2]^-$ (refcode LATGES). In addition there are smaller inorganic complexes, for example $[ReCl_6]^{2-}$ (refcode GEMXAX), $[MnCl_4]^{2-}$ (refcode NAHPOB) and $[W_3S_8]^{2-}$ (refcode DOFMOA). There are slightly more monoanions than dianions (77 *cf.* 59), one trianion (refcode WIPSET) and two tetraanionic species (refcodes TOXTEF and TOXTIJ). However, the salts of the tri- and tetraanions do not contain only $[PPN]^+$ counter ions, but are $[PPN]_2[K(16\text{-crown-}6)][Mo_{12}O_{40}P]$ (refcode WIPSET), $[NBu_4]_2[PPN]_2[Ag_4\{\mu_3\text{-}(CN)_2C_2S_2\}_4]$ (refcode TOXTEF) and $[NBu_4]_2[PPN]_2[Ag_8\{\mu_4\text{-}(CN)_2C_2S_2\}_4\{\mu_3\text{-}(CN)_2C_2S_2\}_2(PPh_3)_4]$ (refcode TOXTIJ). The same chemical diversity applies to the 613 salts not in the motif set, with organometallic carbonyl complexes being the most predominant anions. Thus the close crystal packing of cations arising from supramolecular motifs is not a function of anion size, nature, or charge.

It was not considered appropriate to lengthen the P···P cut-off distance to include a greater proportion of compounds. Our analysis focuses on those structures which display the shorter interactions and thus the driving forces in the formation of the supramolecular assemblies.

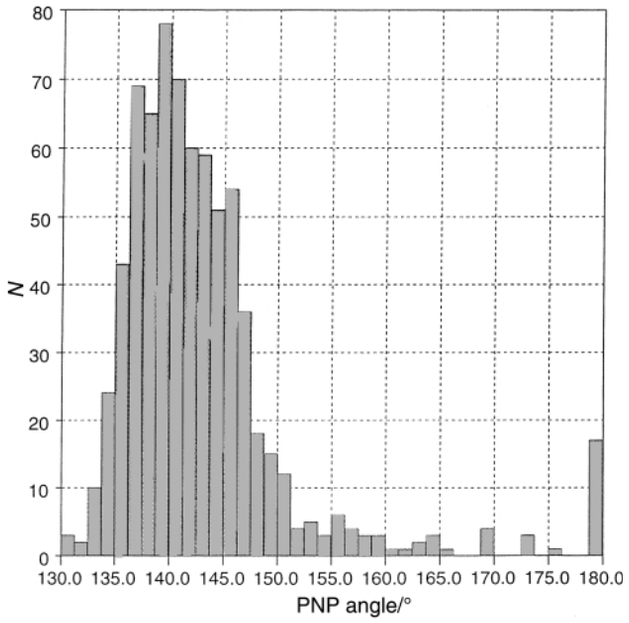

Fig. 2 Histogram of intramolecular P–N–P angle (°) for all $[PPN]^+$ salts.

Intramolecular geometry of the $[PPN]^+$ cation

The intramolecular P–N–P angles for all 752 $[PPN]^+$ salts were examined. The histogram of the angles (Fig. 2) shows that the majority of $[PPN]^+$ cations are bent, with a P–N–P angle between 130 and 150°, and a mean of 143.1°. There is a small but significant number of linear structures (17 in total; only one of the 139 salts in the motif set) which have P–N–P angles of exactly 180°. The histogram of the motif set is analogous to Fig. 2. The geometry of $[H_3PNPH_3]^+$ as a model for the bending of $[PPN]^+$ was investigated using DF calculations, with the potential energy computed for P–N–P angles of between 120 and 180° at 5° increments, giving a relatively flat energy well for the bending. The energy decreases by 1 kcal mol^{-1} from 180° to a very shallow minimum between 145 and 150°, before increasing by more than 2 kcal mol^{-1} at angles smaller than 130°. Therefore the low energy barrier for the flexing of the $[PPN]^+$ cation is consistent with the range of intramolecular P–N–P angles observed in the structures, with the majority of structures having a conformation corresponding to the energy minimum for the molecule.

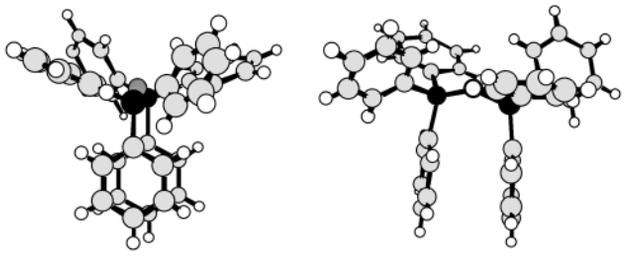

Fig. 3 Two views of the intramolecular **off** arrangement of phenyl rings in the crystal structure of [PPN][$Rh_6(\mu_3\text{-}CO)_4(CO)_{12}Cl$] (CSD refcode KUNBEA).

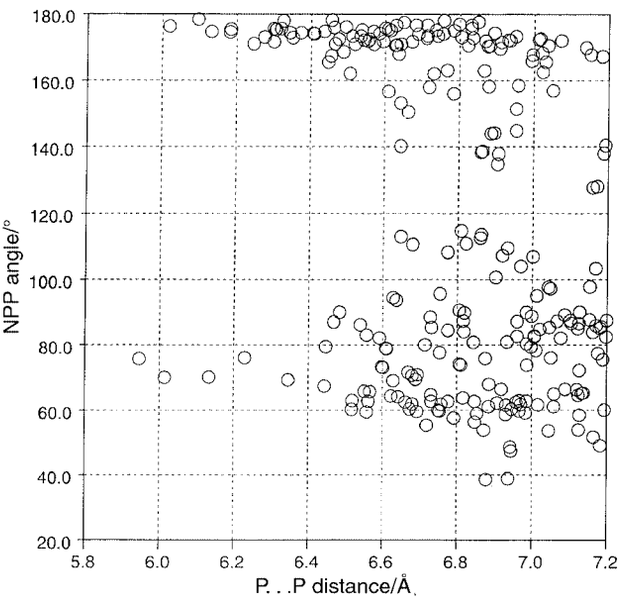

Fig. 4 Scattergram of N–P···P angle (°) *vs.* P···P distance (Å) for selected $[PPN]^+$ salts.

In addition to bending, the cation adopts different conformations according to the rotation of the PPh_3 moieties about the P–N bonds. When the two PPh_3 moieties are eclipsed neighbouring phenyl rings from either end of the $[PPN]^+$ molecule adopt an offset face-to-face (**off**) orientation between the rings if they are sufficiently close and parallel. The intramolecular conformation of phenyl rings may be quantified by (a) the torsion angle between the centroids of adjacent phenyl rings and the two phosphorus atoms, (b) the distance between the centroids, (c) the angle formed by the *ipso*-carbon of one ring, the centroid of the same ring and the neighbouring centroid (the degree of offset), and (d) the angle between the planes of the rings. Of the 139 structures in the motif set, approximately one third have eclipsed rings, with the average centroid separation 3.76 Å, and offset by 1–13°. A good example of this close intramolecular **off** interaction is seen in the cations of [PPN][$Rh_6(\mu_3\text{-}CO)_4(CO)_{12}Cl$] (refcode KUNBEA), in which the adjacent phenyl ring centroids are 3.57 Å apart, the rings 7.4° from parallel and offset by 1.2° (Fig. 3). However, in the majority of structures a combination of separated π systems, non-parallel ring orientations and overlapping of regions of like charge indicates the lack of significantly attractive intramolecular interactions.

Intermolecular interactions

As previously described,[5,6,8] the nature of the interaction between two neighbouring $[XPPh_3]^+$ moieties (X = Ph, Me or M) may be classified by the X–P···P angle, where X is the atom bound to phosphorus but not involved in the interaction. For 6PEs the angle is in the range 160–180°, whilst for offset 6PEs it is in the range 140–160°. A scattergram of the N–P···P angle *vs.* the P···P distance for the 139 $[PPN]^+$ salts in the motif set (Fig. 4) shows three non-intersecting subsets; 91 interactions have the angle 160–180°, 21 interactions have the angle 125–160°, and 142 interactions have angles evenly distributed between 40 and 115°. From the number of instances in each set it is evident that some structures contain more than one intermolecular motif. The almost linear interactions are 6PEs, whilst the more acute interactions arise from multiple phenyl embraces not previously described. These are discussed below.

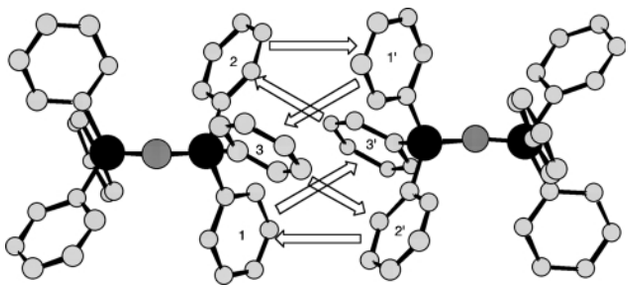

Fig. 5 A representative sixfold phenyl embrace (6PE) in the crystal structure of $[PPN]_2[Ru_5(\mu\text{-}C)(\mu_4\text{-}S)(CO)_{14}]$ (CSD refcode JOYNAM). The arrows signify the six edge-to-face (**ef**) interactions between phenyl rings. Hydrogen atoms have been omitted for clarity.

(a) 6PEs between $[PPN]^+$ cations. The $[PPN]^+$ cations form sixfold phenyl embraces 6PEs. As shown in Fig. 5, the 6PE comprises six phenyl rings of two neighbouring molecules which are involved in significant attractive interactions between the cations. As with the 6PEs described for $[PPh_4]^+$ cations,[5] those observed between $[PPN]^+$ cations comprise six **ef** interactions between phenyl rings. In contrast to the 6PEs observed in $[PPh_4]^+$ salts, where the majority of the interactions have a centre of symmetry midway between the P atoms, the 6PEs occurring between $[PPN]^+$ cations do not lie either side of a crystallographic symmetry site. However, the 6PEs between $[PPN]^+$ cations are characterised by pseudo-centrosymmetry between the embracing cations, with the absence of crystallographic symmetry attributed to the asymmetry of the remainder of the cation and its interactions. The N–P vectors of adjacent cations are approximately parallel and approximately collinear; the scattergram of N–P···P angle *vs.* P···P distance (Fig. 4) shows a distinct concentration of points in the collinearity range 160–180° and the distance range 6.0–7.25 Å, which may be considered 6PE motifs. The majority of N–P···P angles are greater than 170° with the average P···P separation for the 6PEs being 6.67 Å.

(b) Expanded 6PEs involving more than two PPh_3 moieties. In addition to the 6PEs, a second type of intermolecular interaction is observed between $[PPN]^+$ cations, with the N–P···P angle less than 120°, involving six phenyl rings from more than two PPh_3 moieties of two neighbouring cations. These interactions are expanded phenyl embraces, denoted EPEs. There are two markedly different cation pairings that both give rise to similar EPEs: one in which one cation is oriented orthogonally to the PNP plane of its neighbour, denoted OEPE, and a second in which the two neighbouring cations lie parallel to each other, denoted PEPE. The neighbouring cation geometries are illustrated in Fig. 6.

The OEPE (Fig. 7) comprises the three phenyl rings of the PPh_3 moiety from the cation oriented 'end-on' to the embrace (cation A), and three phenyl rings from the two PPh_3 moieties of the 'side-on' cation (cation B). One phenyl group of cation A (ring 3) is directed away from the interaction domain, but is the recipient of an **ef** interaction. There is one **off** interaction between rings 2 and 5, with the remaining rings being engaged in **ef** or **vf** interactions.

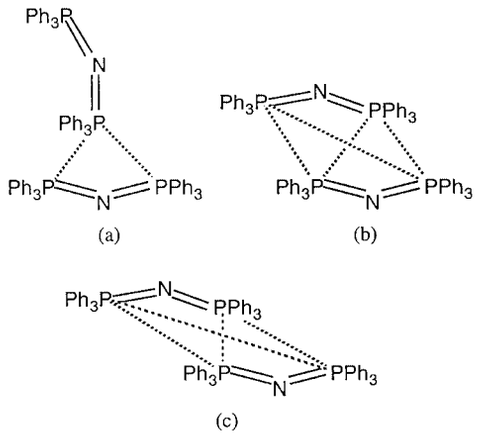

Fig. 6 Cation orientations for expanded phenyl embraces, EPEs; (a) orthogonal, (b) parallel and (c) offset parallel.

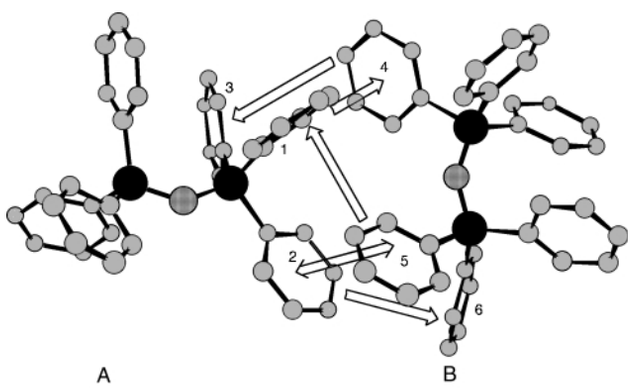

Fig. 7 A representative orthogonal expanded phenyl embrace (OEPE) in the crystal structure of $[PPN]_2[Ru_5(\mu\text{-}C)(\mu_4\text{-}S)(CO)_{14}]$ (CSD refcode JOYNAM). The double arrow signifies an approach of rings 2 and 5 in an offset face-to-face (**off**) interaction; the interaction $2 \Rightarrow 6$ is vertex-to-face (**vf**) with $1 \Rightarrow 4$, $4 \Rightarrow 3$ and $5 \Rightarrow 1$ being edge-to-face (**ef**). Hydrogen atoms have been omitted for clarity.

The PEPE (Fig. 8) comprises three phenyl rings of two PPh_3 moieties from each of the side-by-side cations, and is centrosymmetric. Thus the embrace is essentially a 6PE in which there is a set of six **ef** or **vf** local interactions.

A scattergram of the N–P···P angle *vs.* the P···P distance (Fig. 4) shows a concentration of points in the angle range 40–120° and a distance range 5.95–7.25 Å, all of which are EPE motifs. There is no preference in either N–P···P angle or P···P distance for the OEPE over the PEPE. Whilst the OEPE and PEPE may be differentiated by the N–P···P–N torsion angle, the two embraces are best characterised by inspection of the four intermolecular P···P distances formed by the two neighbouring cations (Fig. 6). A PEPE has three short P···P separations and one long, whilst the OEPE has two short separations and two long. If a PEPE is slightly offset, *i.e.* the two parallel cations are not exactly side-by-side, then one short, two medium and one long P···P distances are observed. Of the 142 instances of expanded embraces, 25 are OEPEs and 117 PEPEs, with 21 of the PEPEs slightly offset.

A closer approach of cations is possible in EPEs, compared to 6PEs, with P···P distances as short as 5.95 Å. However, only five structures display EPEs with a P···P separation of less than 6.4 Å, with the average being 6.89 Å, longer than that of the 6PEs.

(c) Cation–cation interactions with P···P > 7.25 Å. Analysis of the N–P···P angle and the four P···P distances for the salts with P···P separations greater than 7.25 Å gives some insight into the nature of any intermolecular interactions that may occur in the 482 structures outside the motif set. The

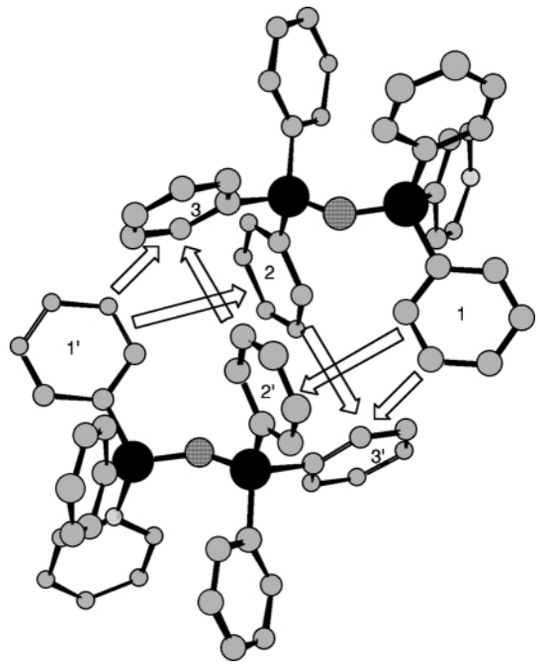

Fig. 8 A representative parallel expanded phenyl embrace (PEPE) in the structure of $[PPN]_2[Ru_{10}(\mu\text{-}CO)_4(CO)_{21}H_2]$ (CSD refcode VIDBOZ). The interactions $3' \Rightarrow 1$ and $1' \Rightarrow 3$ are vertex-to-face (**vf**) with $1' \Rightarrow 2$, $1 \Rightarrow 2'$, $2' \Rightarrow 3$ and $2 \Rightarrow 3'$ being edge-to-face (**ef**). Hydrogen atoms are omitted for clarity.

histogram of N–P···P angle is notably different to that described above; there are far fewer linear cation–cation orientations, with the majority having angles between 60 and 120°, *i.e.* indicating the formation of weak EPEs. Inspection of the intermolecular P···P separations reveals an analogous trend to that observed for the close EPEs, with the PEPE geometry more prevalent than that of the OEPE. However, the PEPEs are generally offset, indicating the absence of a cycle of significant Ph···Ph interactions, *i.e.* the formation of embraces between cations. Subsequently, the upper distance limit for 6PEs and EPEs between $[PPN]^+$ cations may be defined as 7.25 Å. Whilst EPEs are observed over a greater range of intermolecular distances than 6PEs, at P···P distances longer than 7.25 Å the interactions are offset, validating the adoption of this cut-off. At greater separations the conformations adopted by neighbouring cations imply that any interaction is weak and may arise as a consequence of other packing forces.

Interaction energies

The van der Waals and coulombic components of the non-bonded interaction energies between the $[PPN]^+$ cations have been computed by means of standard atom-based calculations for representative examples of each of the motifs 6PE, OEPE and PEPE. These energies are summarised in Table 2, while Table 3 contains the local Ph···Ph energies for one example for each motif.

The **vf**, **ef** and **off** local interactions between phenyl rings in the interaction domains have the expected attractive energies, which range from −0.2 to −1.9 kcal mol^{-1} per pair. These are similar to the comparable interactions in embraces formed by $[PPh_4]^+$ cations.[21] The total attractive energies for the multiple phenyl embraces (Table 2, in kcal mol^{-1} per $\{[PNP]^+\}_2$) are in the ranges −(7.0–10.5) for the 6PE, −(7.9–11.1) for the OEPE, and −(8.6–13.0) for the PEPE. The corresponding energies for multiple phenyl embraces between $[PPh_4]^+$ cations are in the range −(5–11) kcal mol^{-1} per $\{[PPh_4]^+\}_2$.[10] The slightly larger total energies computed for $[PPN]^+$ cations arise mainly from the increased van der Waals component due to the greater number of atoms.

Table 2 Through-space (non-bonded) interaction energies between nearest ions in representative $[PPN]^+$ salts. Total energies (kcal mol^{-1}) are expressed per $\{[PNP]^+\}_2$ cation pair

Motif	Anion	Refcode	P···P/Å	N–P···P/°	Energy/kcal mol^{-1} total	vdW	coul
6PE	$[ReCl_6]^{2-}$	GEMXAX	6.79	174.0	−6.9	−11.7	+4.8
	$[Ru_5(\mu\text{-}C)(\mu_4\text{-}S)(CO)_{14}]^{2-}$	JOYNAM	6.49	178.1	−7.0	−11.3	+4.3
	$[Au\{Co(CO)_4\}_2]^-$	TPCOAU	6.89	177.6	−7.2	−11.3	+4.1
	$[Cu_6Ru_{12}(\mu\text{-}CO)(\mu\text{-}Cl)_2(CO)_{28}]^{2-}$	TUCZEW	6.56	175.2	−8.5	−12.5	+4.0
	$[Cu(N_3)_4]^{2-}$	SEBLUG	6.49	175.9	−8.7	−13.0	+4.3
	$[Mo_6O_{19}]^{2-}$	TERRIR	6.32	175.3	−9.3	−13.3	+4.0
	$[WBr(CO)_3(\eta\text{-}B_{10}C_2H_{10}Me_2)]^-$	YEDTIK	6.11	178.4	−10.5	−14.5	+4.0
OEPE	$[Mo_2(\mu\text{-}O)_2Cl_4O_2]^{2-}$	TINPAH	6.97	109.5	−7.9	−13.0	+5.1
	$[Fe_3Mn(\mu_4\text{-}O)(CO)_{12}]^-$	FIGMUD	6.71	110.6	−9.4	−14.7	+5.3
	$[Cu_6Ru_{12}(\mu\text{-}CO)(\mu\text{-}Cl)_2(CO)_{28}]^{2-}$	TUCZEW	6.92	61.5	−9.5	−14.3	+4.8
	$[Ru_5(\mu\text{-}C)(\mu_4\text{-}S)(CO)_{14}]^{2-}$	JOYNAM	7.00	60.0	−11.1	−15.0	+3.9
PEPE	$[Ru_{10}(\mu\text{-}CO)_4(CO)_{21}H_2]^{2-}$	VIDBOZ	6.64	79.1	−8.6	−12.6	+4.0
	$[Mo(CNMe)(CN)_4O]^{2-}$	KODVOO	5.95	75.8	−12.7	−17.4	+4.7
	$[Mo_6O_{19}]^{2-}$	TERRIR	7.00	62.3	−13.0	−17.8	+4.8

Table 3 Through-space (non-bonded) ring–ring interaction energies (kcal mol^{-1}) between nearest ions in representative $[PPN]^+$ salts. Total energies are expressed per $\{[PNP]^+\}_2$ cation pair. Ph1, Ph2, Ph3, Ph4, Ph5 and Ph6 refer to the six interacting phenyl rings on the neighbouring cations (Figs. 5, 7 and 8)

6PE: CSD refcode JOYNAM; ring numbering in Fig. 5

	Ph1	Ph2	Ph3
Ph1′	−0.03	−1.09	−1.09
Ph2′	−0.84	−0.08	−0.93
Ph3′	−0.84	−0.93	−0.02

OEPE: CSD refcode JOYNAM; ring numbering in Fig. 7

	Ph1	Ph2	Ph3
Ph4	−1.07	−0.67	−1.49
Ph5	−0.20	−1.79	0.07
Ph6	0.21	−1.31	0.37

PEPE: CSD refcode VIDBOZ; ring numbering in Fig. 8

	Ph1	Ph2	Ph3
Ph1′	0.11	−1.85	−0.88
Ph2′	−1.85	−0.13	−0.44
Ph3′	−0.88	−0.44	0.11

As for other polyatomic cations, there is net attraction between $[PPN]^+$ cations because the van der Waals attractions outweigh the net electrostatic energies. As presented in Table 2, the vdW energy for a pair of $[PPN]^+$ cations is in the range −11 to −18 kcal mol^{-1}, while the net electrostatic energy is in the range +3.9 to +5.3 kcal mol^{-1}. It is interesting that the net electrostatic energy calculated for the dispersed single positive charge (Fig. 1) is of similar magnitude to the electrostatic energy calculated for localised charge approximations: representative values (kcal mol^{-1}) are (a) approximation $[N^+]$, E^{coul} = +3.2 (6PE), +5.2 (OEPE), +7.0 (PEPE); (b) approximation $[P^{+0.5}P^{+0.5}]$, E^{coul} = +4.0 (6PE), +5.1 (OEPE), +4.7 (PEPE); (c) approximation $[P^{+0.33}N^{+0.33}P^{+0.33}]$, E^{coul} = +3.7 (6PE), +5.2 (PEPE), +6.2 (OEPE). Our calculation using atom partial charges is more accurate than these approximations, but the approximations serve to demonstrate how the net intermolecular energy between large polyatomic ions of the same charge must be attractive. Rohl and Mingos[24] have previously commented similarly on the balance of van der Waals and coulombic energies for interactions of typical polyatomic cations in crystals. We are unable to find in the literature pertinent experimental data on the association energies for *polyatomic* cations such as $[PPN]^+$, which could be used to refine further the accuracy of the calculated inter-cation energies. There is a question about the general size of the polyatomic cations where inter-cation van der Waals attractions and coulombic repulsions are balanced, and where the net repulsions of smaller cations change to the net attractions of larger cations: this has not yet been addressed.

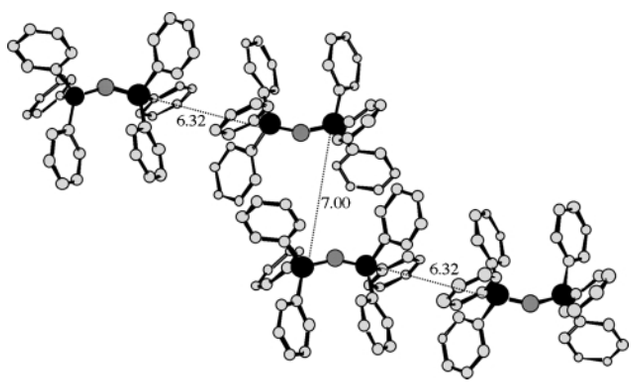

Fig. 9 The chain of alternating 6PEs and PEPEs in the structure of $[PPN]_2[Mo_6O_{19}]$ (CSD refcode TERRIR) with H atoms omitted for clarity. Intermolecular P···P separations (Å) are shown.

Further insight into the preferred conformations of the pairwise embraces is obtained from energy minimisation calculations. In these calculations the intramolecular geometry of the $[PPN]^+$ cation was treated normally using a standard forcefield so that intramolecular as well as intermolecular conformations could change. The minimisations were performed on the representative 6PE, OEPE and PEPE motifs described in Figs. 5, 7 and 8, and Tables 2 and 3. In general there were negligible changes in the motif geometries and energies. The greatest change occurred in the 6PE of JOYNAM, where the net intermolecular energy improved from −7.00 to −8.12 kcal mol^{-1} due to small rotations around P–Ph bonds which improved the quality of the local **ef** interactions.

Crystal packing using these motifs

The intermolecular interactions between pairs of $[PPN]^+$ cations are described above. Here we extend the analysis to the occurrence of these motifs in the three-dimensional crystal structure. The packing details of representative crystal structures are summarised in Table 4. In general, the majority of the structures contain chains of cations, comprising alternating 6PEs and either OEPE or PEPEs, as demonstated by the structure of $[PPN]_2[Mo_6O_{19}]$ (refcode TERRIR) (Fig. 9). There may be subtle variations within the cation chain, for example the 2-D array of cations in the structures of $[PPN]_2[Ru_5(\mu\text{-}C)(\mu_4\text{-}S)(CO)_{14}]$ and $[PPN]_2[Cu_6Ru_{12}(\mu\text{-}CO)(\mu\text{-}Cl)_2(CO)_{28}]$

Table 4 Summary of the crystal structures of 13 representative salts containing $[PPN]^+$ cations

Anion	Refcode	Space group	Anion volume[a]/Å^3	Chain motif[b]	3-D structure	P···P[c]/Å
$[Fe_3Mn(\mu_4\text{-}O)(CO)_{12}]^-$	FIGMUD	$P2_1/c$	359	6···O···6···O···6	Columns	10.1
$[Mo_2(\mu\text{-}O)_2Cl_4O_2]^{2-}$	TINPAH	$P2_12_12_1$	164	6···O···6···O···6	Columns	10.2
$[Au\{Co(CO)_4\}_2]^-$	TPCOAU	$P2_1/c$	247	6···6···6	Columns	11.5
$[WBr(CO)_3(\eta\text{-}B_{10}C_2H_{10}Me_2)]^-$	YEDTIK	$P\bar{1}$	269	6···P···6···P	Columns	9.4
$[Re_6Mo(\mu_6\text{-}C)(CO)_{22}]^{2-}$	ZOVPIJ	$P2_1/c$	677	6···P···6···P	Columns	8.3
$[ReCl_6]^{2-}$	GEMXAX	*Pbca*	160	6···P···6···P···6	Layers	6.8
$[Mn(CO)_5]^-$	JOLWEM	$P\bar{1}$	130	6···P···6···P	Layers	11.0
$[Ru_5(\mu\text{-}C)(\mu_4\text{-}S)(CO)_{14}]^{2-}$	JOYNAM	$P\bar{1}$	451	6···O···P···O···6	Layers	10.0
$[C_6Cl_4O_2]^{2-}$	JUVCEI	$P\bar{1}$	168	6···O···6···O···6	Layers	9.2
$[Mo(CNMe)(CN)_4O]^{2-}$	KODVOO	$P\bar{1}$	176	6···P···6···P···6	Layers	7.7
$[Cu(N_3)_4]^{2-}$	SEBLUG	*Pbca*	131	6···P···6···P···6	Layers	6.5
$[Mo_6O_{19}]^{2-}$	TERRIR	$P\bar{1}$	269	6···P···6···P···6	Layers	10.2
$[Cu_6Ru_{12}(\mu\text{-}CO)(\mu\text{-}Cl)_2(CO)_{28}]^{2-}$	TUCZEW	$P2_1/c$	1170	6···O···P···O···6	Layers	17.1
$[Ru_{10}(\mu\text{-}CO)_4(CO)_{21}H_2]^{2-}$	VIDBOZ	$P\bar{1}$	795	6···P···6···P···6	Layers	16.9

[a] Volumes given by the Connolly surface[23] computed using CERIUS^2,[18] with the volume errors in the range 2–11 Å^3. [b] 6 = 6PE, P = PEPE, O = OEPE. [c] Closest intercolumn/interlayer P···P separation.

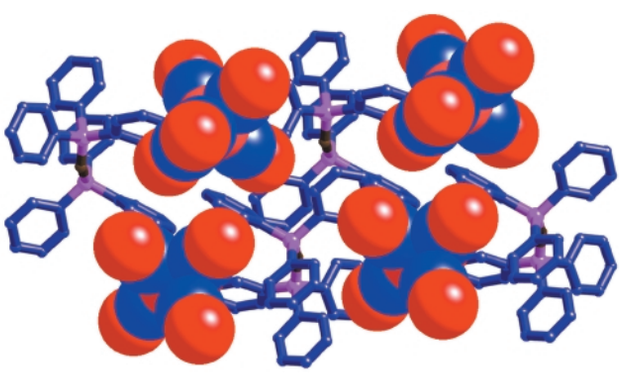

Fig. 10 Crystal structure of $[PPN]_2[Mn(CO)_5]$ (refcode JOLWEM) illustrating the closely packed layers of cations. Hydrogen atoms are omitted for clarity.

(refcodes JOYNAM and TUCZEW respectively) comprise repeating ···6PE···OEPE···PEPE···OEPE···6PE··· units. The repeat distance along the chain is dependent on the combination of intermolecular interactions, ranging from *ca.* 16 Å in the structure of $[PPN][WBr(CO)_3(\eta\text{-}B_{10}C_2H_{10}Me_2)]$ (refcode YEDTIK) to *ca.* 38 Å in the structure of TUCZEW. Owing to the geometries of the intermolecular embraces the chains are not linear, but zigzag slightly with P···P···P angles typically 140–160°. The formation of chains is not dependent on crystal symmetry, nor on stoichiometry, as the 1-D array is observed in monoclinic and triclinic structures, containing mono- or di-anions. The notable exception to the motif of alternating embraces is found in structures such as $[PPN][Au\{Co(CO)_4\}_2]$ (refcode TPCOAU), in which the cations have intramolecular PNP angles of exactly 180°, where the cations form a linear chain of repeating 6PEs. However, of the 139 structures in the motif set, TPCOAU is the only structure to fall into this category.

Two distinct crystal packing arrangements of the cation chains are observed. The more common is one in which chains of cations pack side-by-side to form layers which are sandwiched by layers of anions. Cations of neighbouring chains are separated by intermolecular H···H distances typically 3.0 Å. Thus the $[PPN]^+$ cations only form embraces in the direction of the chain, as opposed to engaging in 2-D supramolecular motifs. The anion layers pack closely to the cations, with many short intermolecular contacts such as O···H–C hydrogen bonds between carbonyl moieties of anions and phenyl rings of the cations. As shown in Fig. 10, the layer structure is well illustrated by $[PPN][Mn(CO)_5]$ (refcode JOLWEM), with the monoanions tightly packed between the anions, with O···H–C interactions typically

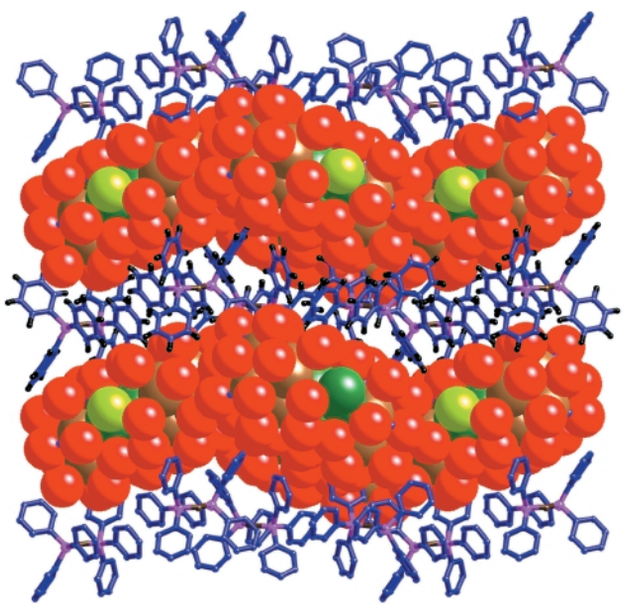

Fig. 11 Crystal structure of $[PPN]_2[Cu_6Ru_{12}(\mu\text{-}CO)(\mu\text{-}Cl)_2(CO)_{28}]$ (refcode TUCZEW) showing the cation layers well separated by the large anions.

2.75 Å, and as short as 2.60 Å. The closeness of cation layers varies with the size of the anion, but does not depend on the stoichiometry of the salt. For example, the cation layers of $[PPN]_2[Cu(N_3)_4]$ (refcode SEBLUG) are separated by P···P distances as short as 6.5 Å, whereas the large $[Cu_6Ru_{12}(\mu\text{-}CO)(\mu\text{-}Cl)_2(CO)_{28}]^{2-}$ dianions of TUCZEW (Fig. 11) cause the cation layers to be much more spaced, with a nearest interlayer P···P distance of 17.1 Å.

The salts that do not have a layer structure form chains of cations, surrounded by four parallel columns of anions, giving a square array. This is well illustrated by the structure of $[PPN][Fe_3Mn(\mu_4\text{-}O)(CO)_{12}]$ (refcode FIGMUD, Fig. 12). As with the formation of 2-D layers, the 1-D chain motif is independent of stoichiometry and crystal symmetry. Although there is a range of anion size, salts containing very small anions do not display this column structure. The chains of cations appear to dominate the crystal lattice, forming a framework around which the anions pack.

Computation of the molecular volumes occupied by the anions, as given by the Connolly surfaces,[23] allows the effect of anion size on the crystal packing to be investigated. The mean volume occupied for the $[PPN]^+$ cation, averaged over the volumes calculated for each of the 13 crystal stuctures in Table 4, is 515(8) Å^3. As seen in Table 4, the anions in the

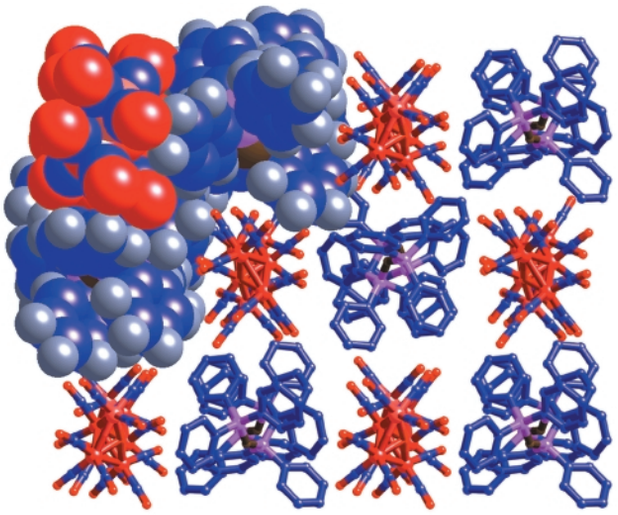

Fig. 12 Columns in the crystal structure of [PPN][$Fe_3Mn(\mu_4$-O)-$(CO)_{12}$] (refcode FIGMUD).

crystal structures studied vary greatly in size, ranging from 131 to 1170 Å^3 for the molecules $[Cu(N_3)_4]^{2-}$ (refcode SEBLUG) and $[Cu_6Ru_{12}(\mu$-CO)$(\mu$-Cl$)_2(CO)_{28}]^{2-}$ (refcode TUCZEW) respectively. Within each packing type, namely columns or layers, there is a wide range of anion volume, indicating that the lattice formation is not dependent on anion size.

Conclusion

We have recognised three recurring supramolecular motifs between $[PPN]^+$ cations, which are denoted 6PE, OEPE and PEPE. The three supramolecular motifs are differentiated by the orientations of the $[PPN]^+$ cations; in the 6PE the cations are end-to-end, the OEPE cations are end-to-side, and the PEPE cations side-by-side. The embraces each consist of sets of individual **ef**, **vf** or **off** interactions between a total of six phenyl rings from the two neighbouring cations. Computation of intermolecular energies for the respective embraces has shown the interactions all to be significantly attractive, with net energies being in the range 7–13 kcal mol^{-1}. Therefore the intermolecular interactions are of similar magnitude to those of the stronger hydrogen bonds.

The pairwise cation embraces extend in the crystal lattice to give zigzag chains of mutually attracted cations. These interactions do not extend to form 2-D and 3-D networks analogous to those observed in salts containing $[PPh_4]^+$ cations. Where the $[PPh_4]^+$ cations can form embraces involving phenyl rings on either side of the phosphorus atom, the linear extension of the $[PPN]^+$ cation increases the separation between embraces. The zigzag chains of cations combine to form either a layer or column structure, with the nature of the cation framework independent of the size, shape or charge of the anion. Similarly, the column structure demonstrates the accommodating nature of the cation lattice; the stacks of counter ions between the chains of cations are either one dianion or two monoanions wide. Therefore the individual cation motifs and the extensions of the motifs to chains, columns and layers are not affected by the properties of the anion.

Of the 752 salts in the CSD only 139 met the selection criterion of intermolecular P···P separations of less than 7.25 Å. Therefore the question remains as to why these 139 structures form arrays of cation embraces and not the others? The nature of the anion will affect the intermolecular interactions in terms of number, type and strength. For example, the oxygen rich surfaces of the organometallic carbonyl clusters may form hydrogen bonds to the positive hydrogen-rich surface of the cations. However, the chemical composition of the salts may be discounted as, by inspection, the diversity of anions is analogous in both the motif set and the discarded structures. Similarly the size of the anions present in the salt is not thought to be responsible as the supramolecular motifs form with both small and large anion complexes. Therefore the structures of the salts which do not have short P···P intermolecular separations, and therefore non-embracing cations, must be dominated by a balance of anion–anion and cation–anion interactions which are energetically favourable over the cation embraces.

Acknowledgements

G. R. L. wishes to thank the Royal Society for a Fellowship tenable overseas. This research is supported by the Australian Research Council.

References

1 J.-M. Lehn, *Angew. Chem., Int. Ed. Engl.*, 1988, **27**, 89; 1990, **29**, 1304.
2 G. R. Desiraju, *The Crystal as a Supramolecular Entity, Perspectives in Supramolecular Chemistry*, ed. J.-M. Lehn, John Wiley, Chichester, 1996; J. D. Dunitz, *Pure Appl. Chem.*, 1991, **63**, 177.
3 F. H. Allen and O. Kennard, *Chem. Des. Automat. News*, 1993, **8**, 131; F. H. Allen, J. E. Davies, J. J. Galloy, O. Johnson, O. Kennard, C. F. MacRae, E. M. Mitchell, G. F. Mitchell, J. M. Smith and D. G. Watson, *J. Chem. Inf. Comput. Sci.*, 1991, **31**, 187.
4 I. G. Dance and M. L. Scudder, *J. Chem. Soc., Chem. Commun.*, 1995, 1039.
5 I. Dance and M. Scudder, *Chem. Eur. J.*, 1996, **2**, 481.
6 C. Hasselgren, P. A. W. Dean, M. L. Scudder, D. C. Craig and I. G. Dance, *J. Chem. Soc., Dalton Trans.*, 1997, 2019.
7 I. Dance and M. Scudder, *New. J. Chem.*, 1998, **22**, 481.
8 M. Scudder and I. Dance, *J. Chem. Soc., Dalton Trans.*, 1998, 329.
9 M. Scudder and I. Dance, *J. Chem. Soc., Dalton Trans.*, 1998, 3155.
10 M. Scudder and I. Dance, *J. Chem. Soc., Dalton Trans.*, 1998, 3167.
11 M. Scudder and I. Dance, *J. Chem. Soc., Dalton Trans.*, 1998, 1341.
12 M. Scudder, H. A. Goodwin and I. Dance, *New J. Chem.*, 1999, 695.
13 T. Palmesen, H. Hoiland and J. Songstad, *Acta Chem. Scand., Ser. A*, 1981, **35**, 803.
14 InsightII, MSI/Biosym Inc, San Diego, 1998, version 4.0.0.
15 A. J. Pertsin and A. I. Kitaigorodskii, *The atom–atom potential method. Applications to organic molecular solids*, Springer Series in Chemical Physics, Springer, Berlin, 1987.
16 A. Gavezzotti, *Theoretical Aspects and Computer Modelling of the Molecular Solid State*, Molecular Solid State Series, John Wiley, Chichester, 1997.
17 A. K. Rappe and W. A. Goddard, *J. Phys. Chem.*, 1991, **95**, 3358.
18 CERIUS^2 molecular modelling software, MSI/Biosym Inc, San Diego, 1998, version 3.8.
19 I. G. Dance, in *The Crystal as a Supramolecular Entity*, ed. G. R. Desiraju, John Wiley, New York, 1996, pp. 137–233.
20 B. F. Ali, I. G. Dance and M. Scudder, in preparation.
21 I. Dance and M. Scudder, *J. Chem. Soc., Dalton Trans.*, 1996, 3755.
22 DMol, MSI/Biosym Inc, San Diego, USA, version 4.0.0; see B. Delley, M. Wrinn and H. P. Lüthi, *J. Chem. Phys.*, 1994, **100**, 5785.
23 M. L. Connolly, *Science*, 1983, **221**, 709; *J. Am. Chem. Soc.*, 1985, **107**, 1118.
24 A. L. Rohl and D. M. P. Mingos, *J. Chem. Soc., Dalton Trans.*, 1992, 3541.

Refcode references

CASRAP. B. F. G. Johnson, J. Lewis, W. J. H. Nelson, J. N. Nicholls, J. Puga, P. R. Raithby, M. J. Rosales, M. Schroder and M. D. Vargas, *J. Chem. Soc., Dalton Trans.*, 1983, 2447.
DOFMOA. S. Bhaduri and J. A. Ibers, *Inorg. Chem.*, 1986, **25**, 3.
FIGMUD. C. K. Schauer and D. F. Shriver, *Angew. Chem., Int. Ed. Engl.*, 1987, **26**, 255.
GEMXAX. C.-N. Chau, R. W. M. Wardle and J. A. Ibers, *Acta Crystallogr., Sect. C*, 1988, 44, 751.
JOLWEM. M. S. Corraine, C. K. Lai, Y. Zhen, M. R. Churchill, L. A. Buttrey, J. W. Ziller and J. D. Atwood, *Organometallics*, 1992, **11**, 35.
JOYNAM. U. Bodensieck, G. Meister, H. Stoeckli-Evans and G. Suss-Fink, *J. Chem. Soc., Dalton Trans.*, 1992, 2131.

KODVOO. H. Arzoumanian, M. Pierrot, F. Ridouane and J. Sanchez, *Transition Met. Chem.*, 1991, **16**, 422.
KUNBEA. A. L. Rheingold, C. B. White, P. D. Macklin and G. L. Geoffroy, *Acta Crystallogr.*, *Sect. C*, 1993, **49**, 80.
LATGES. I. T. Chizhevsky, I. V. Pisareva, P. V. Petrovskii, V. I. Bregadze, A. I. Yanovsky, Yu. T. Struchkov, C. B. Knobler and M. F. Hawthorne, *Inorg. Chem.*, 1993, **32**, 3393.
NAHPOB. P. G. Jones, C. Thone and S. Jager, *Z. Kristallogr.*, 1996, **211**, 657.
SEBLUG. W. Hiller, K. Hosler and K. Dehnicke, *Z. Anorg. Allg. Chem.*, 1989, **574**, 7.
TERRIR. S. Hoppe, J. L. Stark and K. H. Whitmire, *Acta Crystallogr.*, *Sect. C*, 1997, **53**, 68.
TINPAH. C. Limberg, A. J. Downs, A. J. Blake and S. Parsons, *Inorg. Chem.*, 1996, **35**, 4439.
TOXTEF, TOXTIJ. C. W. Liu, C. J. McNeal and J. P. Fackler Junior, *J. Cluster Sci.*, 1996, **7**, 385.
TPCOAU. R. Uson, A. Laguna, M. Laguna, P. G. Jones and G. M. Sheldrick, *J. Chem. Soc.*, *Dalton Trans.*, 1981, 366.
TUCZEW. M. A. Beswick, J. Lewis, P. R. Raithby and M. C. R. de Arellano, *Angew. Chem.*, *Int. Ed. Engl.*, 1997, **36**, 291.
VIDBOZ. P. J. Bailey, E. Charalambous, J. Hoyle, B. F. G. Johnson, J. Lewis and M. McPartlin, *J. Chem. Soc.*, *Chem. Commun.*, 1990, 1443.
WIPSET. R. Neier, C. Trojanowski and R. Mattes, *J. Chem. Soc.*, *Dalton Trans.*, 1995, 2521.
YEDTIK. S. Li, D. F. Mullica, E. L. Sappenfield and F. G. A. Stone, *J. Organomet. Chem.*, 1994, **467**, 95.

Paper a907808h